AIAA JOURNAL
Vol. 31, No. 11, November 1993

Gas Temperature Measurements Using a Dual-Line Detection Rayleigh Scattering Technique

M. Volkan Ötügen*
Polytechnic University, Brooklyn, New York 11201
Kurt D. Annen†
Aerodyne Research, Inc., Billerica, Massachusetts 01821
and
Richard G. Seasholtz‡
NASA Lewis Research Center, Cleveland, Ohio 44135

A new laser-induced Rayleigh scattering method is presented for the improved temperature diagnostics of gas flows. In the present technique, the two lines of a copper vapor laser are used to obtain spatially resolved temperature. A single set of optics is used to form the optical probe and to collect the signal simultaneously from both the 510 nm and the 578 nm lines. The dual-line detection allows for the determination and removal of surface-scattered laser light from the Rayleigh signal, thereby improving the applicability of Rayleigh scattering to near-wall flows with a high degree of glare. An optical system using the dual-line detection technique was built, calibrated, and tested in a hot air jet under various levels of background contamination. The results indicate that accurate temperature measurements are possible even when the laser-line background intensity, captured by the collecting optics, is twice that of the Rayleigh signal.

Nomenclature

C = optical system calibration constant
C' = surface scattering parameter
E_B = detected surface scattered background energy
E_L = laser light energy
E_R = Rayleigh signal energy
E_T = total detected energy
E_0 = incident light energy
L = irradiated length of sample volume
N = photon count
n = gas number density
P = gas pressure
T = temperature
β = ratio of surface scattering constants
ε = efficiency factor
θ = scattering angle
κ = Boltzmann's constant
λ = wavelength of laser light
μ = index of refraction of gas
σ = Rayleigh scattering differential cross-section
σ' = standard deviation
Ω = solid angle of collecting optics
$\langle\rangle$ = mean value

Subscripts
1, 2 = 510 and 578 nm lines, respectively

Introduction

RAYLEIGH scattering is an optical technique that has been successfully used as a temperature and concentration measurement tool in fluid dynamics and combustion research. For example, various researchers used this technique to measure tracer concentration in nonreacting binary gas jets[1–4] and temperature in nonisothermal air jets.[5] The technique has also been applied to simple reacting flows to measure total gas density[6,7] and flame temperatures[8,9] in premixed external flames. Temperature measurements have also been attempted in combustors,[10] but in general these have had limited success due to signal contamination by laser glare. During the last few years, there have been attempts to use Rayleigh scattering for two-dimensional imaging of density and concentration both in subsonic jets[11] and supersonic wind tunnel testing.[12,13] However, high-speed wind tunnel applications for density diagnostics have remained mostly qualitative due to the unwanted scattering of laser light from ice clusters and surrounding surfaces. On the other hand, the application of spectrally resolved Rayleigh scattering as supersonic flow anemometry has been quite successful when the flow velocities are high enough to produce a clearly detectable Doppler shift in scattered signal.[14]

A commonly encountered difficulty associated with the Rayleigh scattering technique is the contamination of the relatively low level of the Rayleigh signal by the background noise. The two major sources of background noise are the contribution of light from the test environment, which is usually broadband, and the surface scattered laser glare captured by the collecting optics along with the Rayleigh signal. Because the Rayleigh line scattered from the gas molecules in the probe volume has approximately the same central frequency as the laser beam, surface scattered light cannot be easily discriminated from Rayleigh scattering, especially in low-speed flows. In certain applications, particularly in enclosed flows with limited optical access such as combustors, surface scattered glare can become a formidable obstacle. The problem becomes most severe when near forward or near backward collecting angles have to be used, because scattering from surfaces and optical elements are larger at these angles.

In the present study, different methods are used to minimize the effects of both types of background contamination. A pulsed copper-vapor laser with a repetition rate of 6 kHz and a continuous output power of 20 W is used as the light source. The use of a pulsed source provides a comparatively high level of Rayleigh signal due to the high energy densities at each pulse and greatly suppresses the effect of environmental noise. However, the improved pulse energy does not help increase the ratio of signal-to-background due to laser glare. A new dual-line detection technique is

Received Oct. 3, 1992; revision received April 10, 1993; accepted for publication April 16, 1993.

*Assistant Professor, Aerospace Engineering Department. Member AIAA.
†Principal Research Engineer, Chemical and Environmental Physics Department. Member AIAA.
‡Research Engineer, Optical Measurement System Branch. Member AIAA.

developed to address this problem. The signal is collected from both the 510 nm (green) and the 578 nm (yellow) lines of the copper-vapor laser using one set of collecting optics. The information obtained from both lines is analyzed together at each shot of the laser to determine the laser line background level and to decouple it from the Rayleigh signal. The dual-line detection method eliminates the need for the guesswork in background determination and offsetting and significantly improves the potential of Rayleigh scattering as a reliable quantitative diagnostic tool in high-temperature gas flows including combustion.

An optical system at NASA Lewis Research Center is used to test the dual-line detection technique. The dual-line detection Rayleigh (DLDR) system uses a copper-vapor laser as the light source. Optical fibers are used to transmit the laser beam to the probe region and the signal to collecting optics. Extensive calibration tests have been performed to characterize the various system parameters. Finally, temperature measurements have been performed successfully in a heated air jet. Results indicate that accurate temperature measurements are possible using the dual-line detection in the presence of high-level background glare. The method for background determination is described in the following section.

Dual-Line Background Detection

Rayleigh scattering involves the elastic interaction of the incident laser light with the gas molecules.[15] The scattered light energy is proportional to the incident laser light energy, the scattering cross-section of the gas, as well as the number density of the gas. Therefore, the technique can be used to measure density directly or temperature by invoking the ideal gas law. The energy of Rayleigh scattered light is given by[16]

$$E_R = E_0\, nL\sigma\Omega\varepsilon \tag{1}$$

For the sampled gas σ is a function of θ, λ, and μ. For an isotropic molecule irradiated by unpolarized light, the Rayleigh cross-section is[17]

$$\sigma = \frac{9\pi^2}{2n^2\lambda^4}\left(\frac{\mu^2-1}{\mu^2+2}\right)^2(1+\cos^2\theta) \tag{2}$$

where n is the molecular number density and θ is defined as the angle between the scattering direction and the propagation direction of the incident light. The value of μ for a gas is typically very close to unity (e.g., $\mu = 1.000293$ for air at $\lambda = 550$ nm at STP). Furthermore, the refractive index term $\mu^2 - 1$ is proportional to number density n of the gas. Therefore, the Rayleigh scattering cross-section can be considered independent of the gas density. For a multispecies gas volume the equivalent (average) cross-section can be found by the weighted average using the mole fraction of each species. Because the Rayleigh cross-section is proportional to λ^{-4}, laser lines with smaller wavelengths result in a stronger signal for unit incident energy. For a given experimental condition with a fixed collecting angle and laser line, the Rayleigh scattered light intensity can be written as

$$E_R = E_L C\sigma n \tag{3}$$

The coefficient C absorbs all of the parameters that are fixed for a given setup. These parameters include the efficiency of the transmitting and collections optics, quantum efficiency of the photomultiplier, and the solid angle over which the signal is collected. However, as discussed in the introduction, the observed signal contains background due to surface scattered laser glare as well as the Rayleigh signal so that

$$E_T = E_R + E_B = E_L C\sigma n + E_L C C' \tag{4}$$

Thus, the relative signal normalized by laser energy is

$$\frac{E_T}{E_L} = C\sigma\frac{P}{\kappa T} + CC' \tag{5}$$

In that equation, the perfect gas law is used. For two-line operation, Eq. (5) can be written for lines λ_1 and λ_2 (with $\lambda_1 = 510$ nm and $\lambda_2 = 578$ nm, in the present case) as

$$\frac{E_{T,1}}{E_{L,1}} = C_1\sigma_1\frac{P}{\kappa T} + C_1C_1' \tag{6}$$

and

$$\frac{E_{T,2}}{E_{L,2}} = C_2\sigma_2\frac{P}{\kappa T} + C_2C_2' \tag{7}$$

For a given optical geometry and electronics setting, the system can be calibrated to obtain the values for C_1, C_1', C_2, and C_2'. This calibration can be accomplished by taking measurements under conditions where the values of σ, P, and T are known, and either one or a combination these known quantities is varied. Therefore, a least squares fit of the data with a sufficient number of conditions determines the constants C_1 and C_2. Furthermore, the ratio $\beta = C_1'/C_2'$ is also obtained through the calibration process. It is reasonable to expect that the scattering process of light from solid surfaces at different wavelengths may be different. However, because the two beams (lines) from the laser are colinear, β should be a constant for a given system. As discussed later, this point is confirmed through experiments using the present DLDR system. Of course, $\beta = 1$ would indicate that the surface scattering is independent of the incident wavelength. With $C' = C_2'$ and $C_1' = \beta C'$, the following is obtained:

$$\frac{E_{T,1}}{E_{L,1}} = \left(\frac{C_1P\sigma_1}{\kappa}\right)\frac{1}{T} + \beta C_1C' \tag{8}$$

$$\frac{E_{T,2}}{E_{L,2}} = \left(\frac{C_2P\sigma_2}{\kappa}\right)\frac{1}{T} + C_2C' \tag{9}$$

Therefore, this linear system of two equations with unknowns $1/T$ and C' yields

$$T = \frac{(P/\kappa)\,(\sigma_1 - \beta\sigma_2)}{(E_{T,1}/E_{L,1})\,(1/C_1) - (E_{T,2}/E_{L,2})\,(\beta/C_2)} \tag{10}$$

and

$$C' = \frac{(E_{T,2}/E_{L,2})\,(\sigma_1/C_2) - (E_{T,1}/E_{L,1})\,(\sigma_2/C_1)}{(\sigma_1 - \beta\sigma_2)} \tag{11}$$

Equation (10) provides the temperature, decoupled from the background contamination. Obviously, this equation can be rearranged for gas density if that property is desired in place of temperature. Equation (11) indicates the normalized background due to surface scattering at the laser lines for each measurement. This information is not related to flow physics; however, in practice, it is important because its magnitude determines if a particular measurement is reliable once a critical threshold value of signal-to-noise ratio is established from preliminary testing. Although Eqs. (10) and (11) completely decouple background from temperature, due to optical and electronic considerations, there is a limiting signal-to-background ratio below which an accurate measurement of temperature is not possible. The present DLDR system was calibrated and tests have been performed to obtain such critical signal-to-noise values.

Uncertainty Analysis

The dual-line Rayleigh scattering technique uses the difference in wavelength dependence between the Rayleigh scattering and the background scattering. The Rayleigh scattering has a λ^{-4} dependence, whereas the background scattering is generally close to wavelength independent. In this section, the uncertainty in gas temperature measurements for each pulse of the laser is analyzed, first for the conventional method based on a single wavelength (line) measurement, and then for the dual-line technique. Because

the main concern is to evaluate the technique as a time resolved temperature probe, only uncertainties due to photon statistics of the measured light are considered. The uncertainty in the measured temperature at each pulse of the laser is expected to be dominated by the photon statistical noise (or photon shot noise) due to low incident light levels.[18]

Single-Line Temperature Measurements

For each of the two wavelengths λ_1 and λ_2 the expected energy of the detected light is given by Eqs. (8) and (9). Assuming the constants C_1, C_2, C', and β are known, each equation can be solved for temperature to yield

$$T = \frac{C_1 \sigma_1 P}{\kappa (E_{T,1}/E_{L,1} - C_1 C' \beta)} \tag{12}$$

and

$$T = \frac{C_2 \sigma_2 P}{\kappa (E_{T,2}/E_{L,2} - C_2 C')} \tag{13}$$

Uncertainty in the temperature measurement is caused by the photon shot noise of $E_{T,1}$ and $E_{T,2}$. The number of detected photons for the two wavelengths are given by

$$\langle N_1 \rangle = \left(\frac{\lambda_1}{hc}\right) E_{T,1} \tag{14}$$

$$\langle N_2 \rangle = \left(\frac{\lambda_2}{hc}\right) E_{T,2} \tag{15}$$

where h is Planck's constant and c is the velocity of light. Because the counts have Poisson statistics, the variance in the number of counts is equal to the expected number of counts.[18] Thus the uncertainties in the counts are

$$\sigma'_{N1} = \langle N_1 \rangle^{1/2} \tag{16}$$

$$\sigma'_{N2} = \langle N_2 \rangle^{1/2} \tag{17}$$

On the other hand, the temperature uncertainties are

$$\sigma'_{T1} = \left(\frac{\partial T}{\partial E_{T,1}}\right) \sigma'_{ET,1} \tag{18}$$

and

$$\sigma'_{T2} = \left(\frac{\partial T}{\partial E_{T,2}}\right) \sigma'_{ET,2} \tag{19}$$

where the energy uncertainties are related to the count uncertainties by $\sigma'_E = (hc/\lambda)\sigma'_N$. Therefore, the relative uncertainties in temperature for each of the two lines are

$$\frac{\sigma'_T}{T} = \frac{1}{1 - [C_1 C' \beta / (E_{T,1}/E_{L,1})]} \left(\frac{1}{(\lambda_1/hc) E_{T,1}}\right)^{1/2} \tag{20}$$

$$\frac{\sigma'_T}{T} = \frac{1}{1 - [C_2 C' / (E_{T,2}/E_{L,2})]} \left(\frac{1}{(\lambda_2/hc) E_{T,2}}\right)^{1/2} \tag{21}$$

Dual-Line Temperature Measurements

In this case, the temperature is described by Eq. (10). If it is assumed that the only source of uncertainty is due to the photon shot noise, then the overall uncertainty in the measured temperature can be written as

$$\sigma'^2_T = \left(\frac{\partial T}{\partial E_{T,1}}\right)^2 \sigma'^2_{ET,1} + \left(\frac{\partial T}{\partial E_{T,2}}\right)^2 \sigma'^2_{ET,2} \tag{22}$$

and the relative uncertainty is

$$\frac{\sigma'_T}{T} = \frac{1}{|(E_{T,1}/E_{L,1})(1/C_1) - (E_{T,2}/E_{L,2})(\beta/C_2)|} \times \left[\left(\frac{E_{T,1}}{E_{L,1}C_1}\right)^2 \frac{1}{(\lambda_1/hc) E_{T,1}} + \left(\frac{E_{T,2}\beta}{E_{L,2}C_2}\right)^2 \frac{1}{(\lambda_2/hc) E_{T,2}}\right]^{1/2} \tag{23}$$

Numerical Example

The following example is presented to illustrate the lower limit of the uncertainty to be expected using the dual-line technique. This uncertainty is compared with the uncertainty of the single wavelength measurements. The parameters used correspond to the calibration data shown in Fig. 7. The detection efficiencies are calculated using the quantum efficiency values provided by the photomultiplier tube (PMT) manufacturer (18% at 510 nm and 15% at 578 nm) and an estimated loss of 50% in the receiving optics. The Rayleigh scattering cross-sections used are those for nitrogen. Calculations are done for two gas temperatures, 300 and 1000 K, with the following values for the parameters used:

$\lambda_1 = 510$ nm;	$\sigma_1 = 7.28 \times 10^{-32}$ m^2 – sr^{-1}
$\lambda_2 = 578$ nm;	$\sigma_2 = 4.37 \times 10^{-32}$ m^2 – sr^{-1}
$E_{L1} = 0.14$ mJ;	$E_{L2} = 0.09$ mJ
$\varepsilon_1 = 0.09$;	$\varepsilon_2 = 0.075$
$T = 300$ K (and 1000 K);	$P = 1$ atm
$f/\# = 2$ ($\Omega = 0.19$ sr)	
$L = 0.2$ mm	

Thus, $C_1 = 0.338 \times 10^5$ m – sr, $C_2 = 0.281 \times 10^5$ m – sr, and $C' = 0.54 \times 10^{-6}$ (m – sr)$^{-1}$. In Fig. 1, the uncertainties in the measurement of gas temperature based on a single laser pulse are plotted as a function of β for the two gas temperatures considered. The effects of signal contamination due to background noise are not included in the single line measurements. Note that the uncertainty for the λ_2 single wavelength is constant, whereas the uncertainty for the λ_1 single wavelength measurement increases with increasing β. This result is a consequence of the way in which the background scattering is defined in Eqs. (8) and (9). The uncertainty of

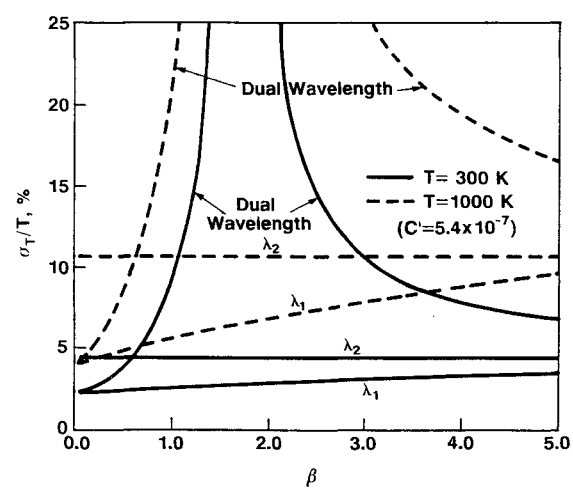

Fig. 1 Relative uncertainty in time-resolved temperature using single wavelength (without background) and dual wavelength techniques.

the single shot dual-line technique has a strong dependence on β, reaching a maximum around $\beta = 1.65$. This condition is where the wavelength dependence of the background surface scattering matches the λ^{-4} wavelength dependence of Rayleigh scattering. In general, it is desirable to have the wavelength dependence of the background scattering differ as much as possible from λ^{-4}. As one would expect, the uncertainties are larger for $T = 1000$ K than those for $T = 300$ K, due to the reduced Rayleigh scattered signal energy obtained at higher temperatures.

The previous analysis is based on the assumption that the photon statistical noise (shot noise) is the dominant source of uncertainty in the temperature measurement. This assumption is generally true when the scattered light levels are low, such as would be the case when measurements are desired for each pulse of the copper-vapor laser. When the scattered light from a large number of laser pulses is averaged, as was done in the experimental work described later, the uncertainty due to photon statistics may no longer be the dominant error source. With averaged data, the relative uncertainty in the mean temperature is reduced by a factor equal to the square root of the number of individual (assumed independent) measurements. In fact, other factors, such as drift in the calibration constants, are the dominant sources of uncertainty when the temperature is obtained by averaging a large number of individual measurements.

Experimental System

The optical arrangement for the dual-line detection Rayleigh scattering system is shown in Fig. 2. Central to the system is a pulsed copper-vapor laser with a continuous power output of about 20 W. The laser is normally operated at a pulse rate of 6 kHz with a pulse duration of approximately 36 ns. The output beam contains both 510 nm (green) and the 578 nm (yellow) lines. The relative power of the 510 nm and the 578 nm lines are approximately 60 and 40%, respectively. The optical probe and the signal collecting optics are situated on an optical bench with a three-axis traverse capability. The laser is placed on a separate optical table, and the output beam is transmitted to the probe bench through an optical fiber. The beam is coupled into the 400-μm fiber by focusing it with a 150-mm focal length lens. The focused beam first passes through a 0.6-mm pinhole for spatial filtering before reaching the cleaved fiber end. The fiber end is placed slightly beyond the minimum waist diameter location so that the fiber end is protected from burning under high incident laser energies. The transmitting optics are composed of two achromatic lenses producing a probe waist of about 400 μm. The incident power at the probe is approximately 1.4 W, although variations did occur on a day-to-day basis. The laser light is captured by a beam trap on the opposite side of the Rayleigh probe. Another light trap is situated directly behind the collecting optics to reduce the broadband background captured by the collecting optics. The collecting optics consist of two achromat lenses, each with a 160-mm focal length and a 80-mm aperture. Therefore, the magnification factor of the collecting optics is unity. The collected signal is coupled into a 200-μm core diam optical fiber and delivered into a sealed signal box. In the signal box, the total collected signal is collimated and subsequently color separated by a dichroic beam splitter. The green (510 nm) and the yellow (578 nm) signals are directed onto two PMTs.

Because the copper-vapor laser used has a significant pulse-to-pulse energy variation (up to 5%), the intensity of the laser from two lines is monitored at each pulse, and the signal is normalized by these values as required by Eqs. (8) and (9). This normalization is accomplished by placing a thin glass plate at a small angle in front of the laser beam as shown in Fig. 2 and reflecting approximately 10% of the beam energy. Some of the reflected laser light is then captured by the open end of a 200-μm core diam fiber. At the other end of the fiber, this reference intensity is delivered to another box configured very similarly to the signal box. The only difference is that the signal in the reference box is sensed by photodiodes instead of PMTs.

The electronic arrangement for the DLDR system is shown in Fig. 3. The set of four sensor outputs for the two lines, the two signals from the PMTs, and the two laser reference intensities from the photodiodes are fed into linear sample and hold units on a boxcar averager system, as shown. The signal from the PMTs is fed directly to the gated integrators without any need for preamplification because a fairly strong Rayleigh signal is observed at each pulse of the laser. The timing for the gate generators is provided by a timing module. The timing module, which is a function generator with a TTL output, also provides the trigger pulses for the copper vapor laser and a 16-bit analog-to-digital converter. The trigger pulses to the gate generators and to the A/D converter are appropriately delayed to capture the Rayleigh scattering signal from the probe. The A/D converter is interfaced with an 80486 personal computer. At each pulse of the laser, all four signals are gated, integrated, digitized, and stored on the hard disk of the computer. Therefore, the system can obtain data at a rate of 6 kHz with a time resolution of about 36 ns. Data is postprocessed after each experiment or calibration on the same personal computer.

Experimental Results

Preliminary tests were performed first to ensure proper operation of the optical and the electronic components of the DLDR system for both the green λ_1 and the yellow λ_2 lines. Temperature was

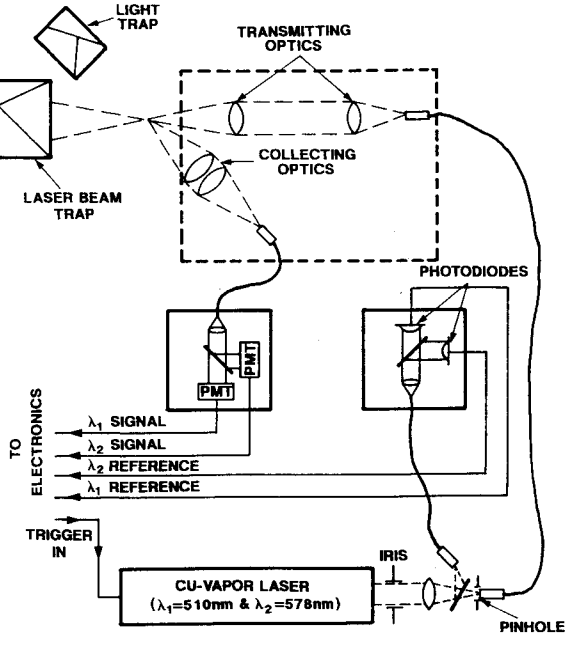

Fig. 2 Optical arrangement for the DLDR system.

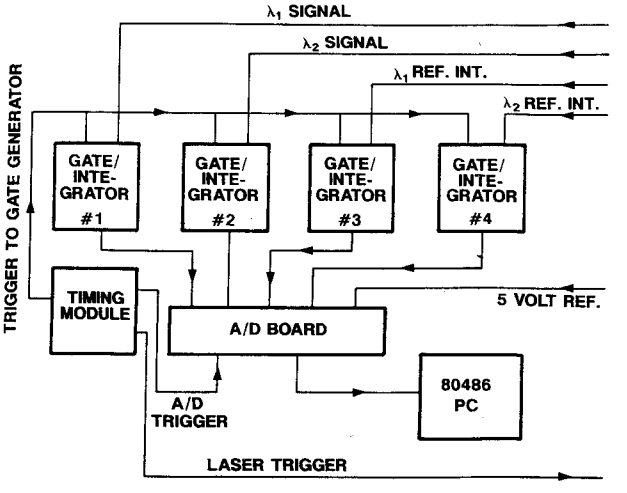

Fig. 3 Electronic arrangement for the DLDR system.

measured in a particulate free, heated air jet. For these measurements the dual-line detection feature was not implemented, and temperature, independently measured from each laser line, was compared to a thermocouple measurement. Both the environmental background and the laser glare were kept to a minimum. For these measurements, the knowledge of the Rayleigh cross-section was not needed a priori. Each line was calibrated using a reference condition (free air jet at room condition), which is the usual method in the more conventional applications of Rayleigh scattering.[2,5] The optical probe was situated on the axis of a jet approximately 1 mm above the nozzle (10 mm diam). A chromel-alumel thermocouple with a nominal bead diameter of 1 mm was placed directly above the Rayleigh probe. Readings from both the Rayleigh scattering system and the thermocouple were obtained at various jet temperatures. Figure 4 shows a typical set of results. In the figure, a straight line with slope of one is also drawn for better comparison. There is good agreement between the thermocouple and the Rayleigh scattering measurements. The slightly higher temperature readings independently obtained by both lines of the Rayleigh system are possibly due to the positioning of the thermocouple relative to the optical probe: the optical probe was slightly closer to the jet exit. (The jet did not have a potential core, and mixing on jet axis started almost immediately downstream of the exit.)

Two separate software routines were developed for the DLDR system: one for calibration and another for actual temperature measurements. The system has to be calibrated each time an experiment is performed because the constants in Eqs. (8) and (9) are highly dependent on optical alignment and electronic settings (laser power, PMT sensitivity, electronic gain, gate width on signal integration, etc). Once the calibration procedure is completed, the relevant constants are put in the data acquisition software. At this point, any change on the electronics setting, including significant electronic drift, would invalidate the calibration.

System Calibration

To qualify the DLDR system, a large set of calibration tests was performed under a diverse set of conditions related to both the optics and the electronics, including the laser power, PMT sensitivities, signal gain, etc. Also, different levels of background were allowed to contaminate the signal during these tests to study the behavior of β. The calibration software essentially acquires data

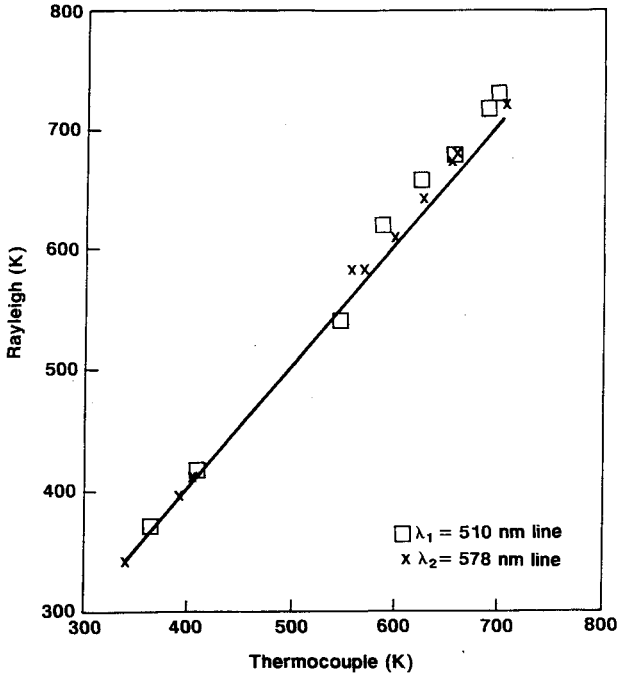

Fig. 4 Temperature obtained by Rayleigh scattering and thermocouple.

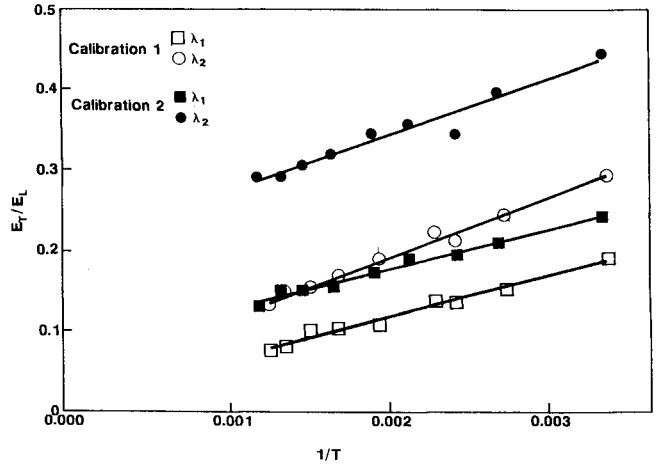

Fig. 5 Calibration curves with various levels of background contamination.

Table 1 Summary of calibration study

	$C_1(\times10^{-4})$	$C_2(\times10^{-5})$	$C_1'(\times10^{7})$	$C_2'(\times10^{7})$	β
Calibration 1	4.472	1.096	2.929	3.300	0.887
Calibration 2	4.481	0.994	14.24	16.20	0.880
Calibration 3	4.566	1.030	15.24	18.93	0.810
Calibration 4	4.441	1.022	18.19	18.98	0.958
Average	4.425	1.048	—	—	0.885
Standard deviation	0.154	0.036	—	—	0.060
Percent deviation	3.5	3.4	—	—	6.78

from both lines and performs a least squares fit to Eqs. (8) and (9). Values of σ, P, and T are provided to the program and depending on the experimental conditions, either one or a number of these parameters can be varied. In the present calibration studies, the heated air jet previously described was used. The Rayleigh scattering cross-sections and pressure (atmospheric) were provided to the software code as fixed values and the air temperature was the calibration variable. The optical probe was placed at the exit of the jet, and the jet temperature was varied. The temperature was monitored by a small-bead, chromel-alumel thermocouple, which was placed adjacent to the optical probe.

Four sets of calibration graphs were obtained during a day with various laser line contamination levels. Two such calibrations are shown in Fig. 5. The background contaminations were obtained by placing painted (with flat black paint) and nonpainted aluminum plates near the Rayleigh optical probe, directly opposite from the collecting optics (Fig. 2). Different levels of background were obtained by moving the small, flat aluminum plates toward and away from the probe location on a traverse mechanism and allowing the diffuse laser light around the probe location to shine on the plates. The diffuse laser light, surrounding the high intensity beam waist (at the probe) is generated by the focusing lens. The coefficients obtained for each of the four calibrations performed are summarized in Table 1. The plots for both laser lines are linear, confirming Eqs. (8) and (9). Also, for a given laser line, the slope of the plot is fixed for various background levels (Table 1). The two sets of calibrations presented in Fig. 5 show two quite distinct background levels. Higher levels of background contamination simply lead to larger offset (y-intercept) in the plots. Furthermore, the values of C_1 and C_2 essentially remain constant throughout the experiments. The amount of fluctuation in these values is a measure of the accuracy of the calibration process. As the surface scattered background noise is increased, the values for the constants C_1' and C_2' progressively increase. However, the most significant result here is the fact that, as postulated, $\beta = C_1'/C_2'$ remains nearly constant throughout the calibrations, although higher signal contamination by the surface scattered background leads to larger values of both C_1' and C_2'. The comparatively high value of β for calibration 4 on Table 1, which represents the calibration with the

largest background contamination level, is believed to be related to the photomultiplier noise levels. A slightly higher background value than that corresponding to this background level led to the saturation of both photomultiplier tubes. This set a limit on the total acceptable signal. The average values for the calibration constants for the same day are also summarized in Table 1. The average value of β is 0.885 with a standard deviation of about 0.06. Note that these calibration results are obtained with nine data points on each calibration curve. A larger number of data points is likely to lead to a lower standard deviation on the constants.

Temperature Measurements

Next, temperature was measured in a clean (particulate free) heated air jet with a coflow. Figure 6 shows the coflow jet apparatus. The coflow was added to the inner jet to prevent the entrainment of particulates from the laboratory environment. Excessive amounts of particulates in the probe region can prevent accurate measurements by contaminating the Rayleigh signal by Mie scattering from those large particles. Only the central jet is heated, and jet exit temperatures in excess of 800 K could be obtained with this apparatus. Again, a thermocouple was situated adjacent to the Rayleigh probe on the downstream side. The thermocouple readings provide a comparison to the DLDR measurements.

Figure 7 shows the calibration results for the experiment. This time, the calibration is performed using 16 points. Because C_1 and

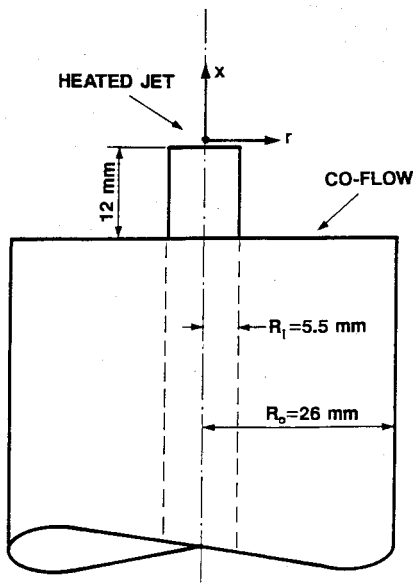

Fig. 6 Heated jet setup with coflow.

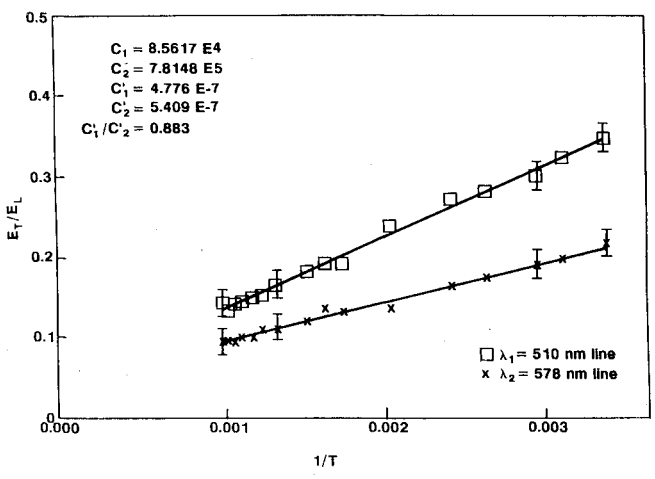

Fig. 7 Calibration curve for the temperature measurements.

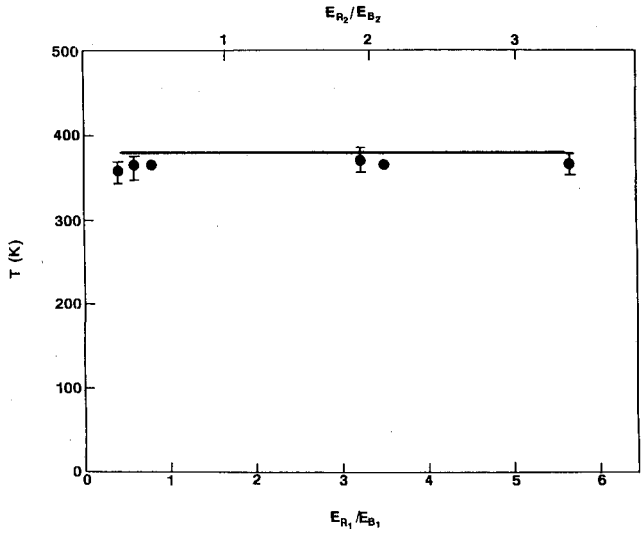

Fig. 8 Temperature measurements under various background levels (T_{jet} = 380 K).

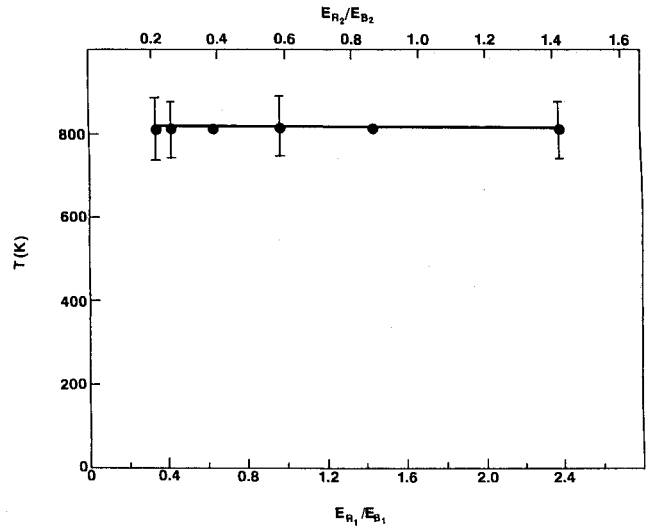

Fig. 9 Temperature measurements under various background levels (T_{jet} = 805 K).

C_2 depend on the electronic and optical settings, the current values are different than those previously obtained (shown in Table 1). However, as expected, the value for β is almost identical to the average value previously obtained. In the figure, estimated error margins are also included at selected points.

The temperature obtained by the DLDR system approximately 2 mm above the exit plane is shown in Figs. 8 and 9 for jet temperatures of 380 and 805 K. The solid line indicates the reading from the thermocouple. For a given heating level of the jet, DLDR measurements are obtained in the presence of various background levels. The background levels were created using the method described earlier. For each background level, the mean temperatures were obtained by averaging readings obtained from 15,384 shots of the laser. This value corresponds to a total sampling duration of about 2.6 s. Data is presented in terms of signal-to-background ratio obtained from both λ_1 and λ_2 lines. E_R/E_B ratios are obtained in the following manner: E_R is calculated from Eqs. (8) and (9), including only the first term on the right-hand side and using the temperature reading from the thermocouple. E_B is obtained directly from the measurements using Eq. (11). The agreement between the DLDR and the thermocouple results is quite good. Particularly encouraging is the fact that even with signal-to-background levels as low as $E_{R,1}/E_{B,1} = 0.5$ (or $E_{R,2}/E_{B,2} = 0.2$), reliable temperature measurements are possible. Note that the lower limit on the signal-

to-noise ratio that appears in Figs. 8 and 9 was determined by a practical consideration: beyond a certain position of the scattering surface, the background level increases sharply and saturates either the sensors or the electronic integrators, rendering measurements impossible beyond that point.

Also included in Figs. 8 and 9 are the standard deviations for each measurement. Because the measurements are made at the jet centerline and close to the exit plane, the turbulent fluctuations of temperature are small, and thus their contribution to the standard deviation is minimal (estimated to be less than 3%). Therefore, as discussed earlier, the bulk of the contribution to the relative uncertainty comes from the photon shot noise. There is essentially no systematic dependence of measurement uncertainty on the background level E_B. However, larger standard deviations are observed for the higher measured temperature (T = 805 K). The averaged, relative standard deviation values obtained for jet temperatures of 380 and 805 K are 6 and 18%, respectively. These compare favorably with the previously estimated uncertainties due to shot noise with $\beta = 0.88$ (Fig. 1). Because the relative uncertainty due to shot noise is inversely proportional to the square root of detected energy, these uncertainty limits on the shot-to-shot temperature measurements would significantly improve with the use of higher pulse energy lasers such as Nd:YAG lasers. With such lasers, pulse energies of 500 mJ are possible as compared to the 0.23 mJ of total pulse energy obtained at the probe location of the current system.

Conclusions

A laser-induced Rayleigh scattering system is developed for gas temperature measurements. A dual-line detection technique is used for the effective detection and removal of the laser line glare from the Rayleigh signal. The technique involves the collection of signals from two lines of a laser. The two linear equations thus obtained are solved simultaneously to give temperature (or density) and the background level. The robustness of the system depends on the difference in wavelength dependence between the Rayleigh scattering and the background scattering. In the present work, a pulsed copper-vapor laser is used as the light source. The 510 nm and the 578 nm lines intrinsic to the laser provide the necessary two lines. The use of a pulsed laser with relatively high pulse energies significantly reduces the effect of broadband background from the surroundings. An analysis based on the photon arrival statistics shows that uncertainty limits in the time-resolved temperature measurement depend on the parameter β. The relative error margins estimated by the analysis for the system agree fairly well with the measurements. Time-averaged results, on the other hand, indicate a high degree of accuracy in temperature measurements. Calibration tests and actual temperature measurements also indicate that the dual-line detection technique can improve the capability of the Rayleigh scattering method by significantly reducing the effect of signal contamination due to laser glare. It eliminates the need for background mapping and the associated guesswork typical of Rayleigh scattering measurements in optically nonideal situations. Accurate temperature measurements were obtained in a heated air jet even when the background level was twice the Rayleigh signal based on the green (510 nm) line. Using the dual-line detection technique, it is hoped that effective Rayleigh scattering measurements in enclosed test sections (such as in combustors with limited optical access) as well as near walls (such as in boundary-layer studies) will be possible. Currently, a second DLDR system, similar to the one discussed here, is being developed that uses an Nd:YAG laser. In this new system, second and fourth harmonics of the laser output will be used as the two detection lines.

Acknowledgments

The present work, which is a continuation of an earlier work at Aerodyne Research (NASA contract NAS3-24613), was undertaken while the first author was a summer faculty fellow at NASA Lewis Research Center, Optical Measurement Systems Branch. The support through NASA Grant NAG-3-1301 is also acknowledged.

References

[1]Graham, S. C., Grant, A. J., and Jones, J. M., "Transient Molecular Concentration Measurements in Turbulent Jets," *AIAA Journal,* Vol. 12, No. 8, 1974, pp. 1140–1143.

[2]Dyer, T. M., "Rayleigh Scattering Measurements of Time-Resolved Concentration in a Turbulent Propane Jet," *AIAA Journal,* Vol. 17, No. 8, 1979, pp. 912–914.

[3]Pitts, W. M., and Kashiwagi, T., "The Application of Laser-Induced Rayleigh Scattering to the Study of Turbulence Mixing," *Journal of Fluid Mechanics,* Vol. 141, April 1984, pp. 391–429.

[4]Arcoumanis, C., "A Laser Rayleigh Scattering System for Scalar Transport Studies," *Experiments in Fluids,* Vol. 3, No. 2, 1985, pp. 103–108.

[5]Ötügen, M. V., and Namer, I., "Rayleigh Scattering Temperature Measurements in a Plane Turbulent Air Jet at Moderate Reynolds Numbers," *Experiments in Fluids,* Vol. 6, No. 7, 1988, pp. 461–466.

[6]Bill, R. G., Jr., Namer, I., Talbot, L., and Robben, F., "Density Fluctuations of Flame in Grid Induced Turbulence," *Combustion and Flame,* Vol. 44, 1982, pp. 277–285.

[7]Gouldin, F. C., and Halthore, R. N., "Rayleigh Scattering for Density Measurements in Premixed Flames," *Experiments in Fluids,* Vol. 4, No. 3, 1986, pp. 269–278.

[8]Dibble, R. W., and Hollenbach, R. E., "Laser Rayleigh Thermometry in Turbulent Flows," *Proceedings of the Eighteenth Symposium on Combustion,* The Combustion Institute, Pittsburgh, PA, 1981, pp. 1489–1499.

[9]Namer, I., and Schefer, R. W., "Error Estimates for Rayleigh Scattering Density and Temperature Measurements," *Experiments in Fluids,* Vol. 3, No. 1, 1985, pp. 1–9.

[10]Barat, R. B., Longwell, J. P., Sarofim, A. F., Smith, S. P., and Bar-Ziv, E., "Laser Rayleigh Scattering for Flame Thermometry in a Toroidal Jet Stirred Combustor," *Applied Optics,* Vol. 30, No. 21, 1991, pp. 3003–3010.

[11]Escoda, C., and Long, M. B., "Rayleigh Scattering Measurements of Gas Concentration Field in Turbulent Jets," *AIAA Journal,* Vol. 21, No. 1, 1983, pp. 81–84.

[12]Smith, M., Smits, A., and Miles, R., "Compressible Boundary Layer Density Cross Sections by UV Rayleigh Scattering," *Optics Letters,* Vol. 14, No. 17, 1989, pp. 916–918.

[13]Shirinzadeh, B., Hillard, M. E., and Exton, R. J., "Condensation Effects on Rayleigh Scattering Measurements in Supersonic Wind Tunnel," *AIAA Journal,* Vol. 29, No. 2, 1991, pp. 242–246.

[14]Seasholtz, R. G., and Zupank, F. J., "Spectrally Resolved Rayleigh Scattering Diagnostics for Hydrogen-Oxygen Rocket Plume Studies," *Journal of Propulsion and Power,* Vol. 8, No. 5, 1992, pp. 935–942.

[15]Van de Hulst, H. C., *Light Scattering by Small Particles,* 1st ed., Chapmann & Hall, London, 1957, pp. 63–83.

[16]Jenkins, F. A., and White, H. E., *Fundamentals of Optics,* 4th ed., McGraw-Hill, New York, 1981, pp. 471–473.

[17]McCartney, E. J., *Optics of the Atmosphere,* 1st ed., Wiley, New York, 1976, pp. 187–196.

[18]Goodman, J. W., *Statistical Optics,* Wiley, New York, 1985, pp. 466–470.